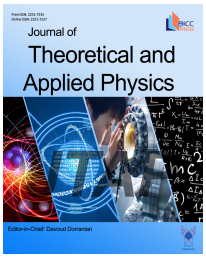


Volume 18, Issue 1, 182410 (1-11)

Journal of Theoretical and Applied Physics (JTAP)

https://dx.doi.org/10.57647/j.jtap.2024.1801.10

# Improving the terahertz collection efficiency based on impedance matching in spintronic THz emitters

Seyedeh Maryam Hosseini, Amin Sadraei Javaheri, Fazel Jahangiri, Seyedeh Mehri Hamidi*, Hamid Latifi

*Laser and Plasma Research Institute, Shahid Beheshti University, Tehran, Iran.*

***Corresponding author:** m_hamidi@sbu.ac.ir

**Original Research**

Received:
17 October 2023
Revised:
15 November 2023
Accepted:
27 November 2023
Published online:
10 January 2024

**Abstract:**

We study the improvement of terahertz collection efficiency in a THz-TDS system based on a spintronic THz emitter, by exploring the effect of substrate impedance matching. This improvement is obtained by properly coupling a hyper-hemispherical lens fabricated from suitable THz materials to a non-magnetic (NM)|ferromagnetic (FM)|substrate emitter structure. The emitter is a Ni|Pt bilayer film coated on a MgO substrate. The refractive index and the dispersion properties of the substrate are adjusted according to the impedance matching conditions and consequently for the maximum THz collection efficiency by a photoconductive antenna (PCA). By comparing various substrates, including MgO, $Al_2O_3$, $SiO_2$, and polyethylene terephthalate (PET), our results reveal that the power of the THz radiation collected from the Ni|Pt|MgO with the hyper-hemispherical Si-lens coupler is 64.5 times larger than that from the Ni|Pt|MgO without the lens coupler. A PET substrate in direct contact with a hyper-hemispherical Teflon-lens could be a favorable choice for improved collection efficiency of STE-induced THz radiation, in the absence of Si-lens. These results could be considered useful to achieve the guidelines for scaling the THz radiation power emitted from the spintronic THz emitter according to the employed substrate and hyper-hemispherical lens.

**Keywords:** THz-TDS; Spintronic THz emitter; Index-matching; Hyper-Hemispherical lens

## 1. Introduction

Terahertz (THz) waves with a frequency range of 0.1 to 30 THz have provided rich application fields such as spectroscopy [1], sensing [2, 3], security monitoring [4], military [5], and communication [6]. Due to the low photon energy, THz radiation is not harmful to the human body and can be used for medical diagnostics and treatments [7–9]. Broadband THz pulses can be generated via optical rectification and parametric oscillation in nonlinear crystals and photoconduction in semiconductors via the ultrafast femtosecond laser pulse [10–16]. THz time-domain spectroscopy (THz-TDS) could be considered as useful diagnostic tool in spintronics for studying dynamics of ultrafast carriers (spin and charge) and gaining a deeper understanding of the behavior of materials at THz frequencies [17]. These frequencies correspond to various physical phenomena, including spin precession spanning from one picosecond to one nanosecond, electron spin-orbit interaction ranging from 0.1 to 1 picoseconds [18], and exchange interaction occurring within a timeframe of 0.01 to 0.1 picoseconds [10, 11, 19] The synergistic integration of spintronics and THz technology offers novel prospects for investigating uncharted territories. In this case, spin-dependent electronic emitters as a novel source of THz were proposed to generate the ultra-broadband THz emission. Two- and three-layer spintronic structures, comprising ferromagnetic (as spin source) and non-magnetic (as spin sink) nanometer layers, have been recently studied as potential high power and high bandwidth THz emitters, known as spin-based THz emitters (STEs) [20–23]. The key factors motivate the enhancement of THz radiation power are the increase in transient current induced by ultrashort laser pulse excitation through the magnetic-field tailoring [10] or reduction in temperature [24], as well as the reduction in energy loss during THz ra-

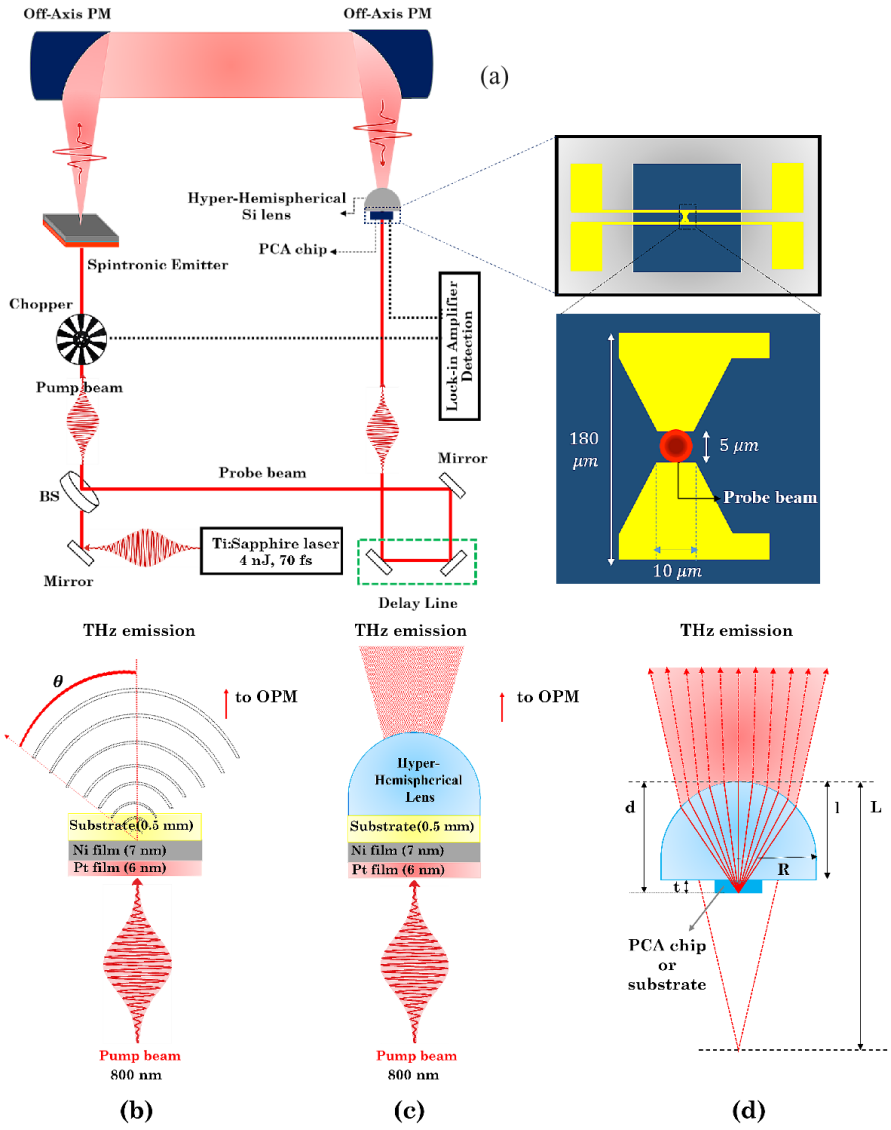


**Figure 1.** Schematic illustration of (a) the THz-TDS experimental setup, and full top view of a photoconductive antenna chip, as well as, extended top view of the midway placed THz dipole structure only displaying antenna length, gap distance, and gap width; STE-induced THz divergence profile (b) without lens attachment as a reference and (c) with the hyper-hemispherical lens attachment on off-axis parabolic mirror; $\theta$ is considered cone angle in COMSOL simulation. (d) The dimensions of the hyper-hemispherical lens in accordance with the parameters presented in Table 2.

diation propagation [25]. The THz electric field amplitude ($E_{THz}$) is related to the charge current ($j_c$) and the effective impedance of the STE ($Z_{eff}(\omega)$) as $E_{THz} = j_c.Z_{eff}(\omega)$ [26]. The effective impedance of the STE depends on the refractive index of the substrate and the conductivity of the STE [27]. According to the theory of impedance matching, the refractive index of the lens and substrate of STE should be same to avoid the losses at the substrate/lens interface when the femtosecond laser pulse is incident from the non-magnetic side [26]. Efficient THz source development is impeded by significant diffraction at the substrate surface of the emitter for radiated THz waves due to refractive index difference, which also renders detection challenging. Refractive index matching has the potential to enhance the collection efficiency of THz radiation from spintronic THz emitters. Optical elements employed for guiding THz waves between the emitter and detector in THz-TDS systems, including lenses and off-axis parabolic mirrors play a crucial role in index-matching. Improved collection efficiency of THz radiation can be achieved by employing commonly THz lenses fabricated from a range of materials, including high-resistive float zone (HRFZ) silicon [23, 28, 29], polytetrafluoroethylene (PTFE, Teflon) [30–32], high-density polyethylene (HDPE) [31, 33], and polymethyl pentene (TPX) [31]. The utilization of hyper-hemispherical lenses has been proposed to effectively collect the THz beam divergently radiate from the emitter and subsequently focus on the detection antenna [28, 34–40]. The efficacy of hyper-hemispherical (HH) lenses in reducing radiation divergence and enhancing the performance of optical systems makes them a valuable tool for light manipulation.

In this work, we study the effect of substrate impedance

**Table 1.** Summary of the detailed steps of pre-ray tracing, ray tracing, and post-ray tracing technique in COMSOL.

| **Step** | **Model Builder** | | |
|---|---|---|---|
| 1 | Global definitions | Define parameters<br>Geometry part: paraboloidal reflector 3D | |
| 2 | Component | Geometry objects | |
| | | Materials | Substrates: MgO, $Al_2O_3$, $SiO_2$, PET<br>Hyper-hemispherical lens: Si, PTFE<br>Parabolic mirrors: Silver<br>PCA chip: Semi-insulating GaAs |
| | | Geometrical optics | Release from point:<br>Number of rays in wave vector space=20000<br>Cone angle = $\pi$/4.5 (rad) |
| | | Mesh | Physics-controlled mesh<br>Element size: extremely fine |
| 3 | study | Ray tracing | |
| 4 | Results | Dataset<br>3D plot & Export data | Intersection point |

matching in a spintronic THz emitter on the improvement of THz collection efficiency in a THz-TDS system. The emitter is a Ni|Pt bilayer thin film coated on a MgO substrate properly coupled to a hyper-hemispherical lens fabricated from suitable THz materials. We present the results for various lens materials including high-resistive float zone (HRFZ) silicon and polytetrafluoroethylene (PTFE, Teflon) as well as various substrates, including MgO, $Al_2O_3$, $SiO_2$, and polyethylene terephthalate (PET). We also discuss the role of index-matching between the substrate and hyper-hemispherical lens coupler on the THz emission power by using the finite element method. Through simulations, THz ray accumulation resulting from a STE grown on various substrates, including MgO, $Al_2O_3$, $SiO_2$, and PET on a PCA chip are compared. It has been shown that the optimization of THz radiation collection can be achieved by using a MgO substrate with a hyper-hemispherical Si-lens coupler. Our results reveal that the power of the THz radiation collected from the Ni|Pt|MgO with the hyper-hemispherical Si-lens coupler is 64.5 times larger than that from the Ni|Pt|MgO without the lens coupler. Moreover, the use of a PET substrate with a hyper-hemispherical Teflon-lens coupler could provide a favorable environment for improved collection efficiency of THz radiation, in the absence of Si-lens.

## 2. Methods and materials

### 2.1 Experiment

In the pursuit of creating a high-performing bilayer nanostructure, a metallic bilayer was skillfully deposited onto a 0.5-mm-thick MgO substrate using a sputtering system. The bilayer itself consisted of a 7-nanometer-thick ferromagnetic layer of Ni that was thoughtfully capped with a 6-nanometer non-magnetic layer of Pt. Sputter parameters for the system were a base pressure of $5 \times 10^{-3}$ mbarr and a sputtering deposition time of about 30 min. The rotational speed of the substrate was 20 rpm. In this system, the applied voltage between the cathode and anode, and the distance between them are about $270 - 300$ volt and 20 cm, respectively. The experimental schematic diagram for the THz beam generation is plotted in Fig. 1(a), which consists of the Ni|Pt-based emitter and photoconductive antenna detection system. A femtosecond commercial nJ Ti:sapphire laser pulse as a heart of set-up produces optical pulses with a power of about 400 mW, time duration of 70 fs, and repetition rate of 100 MHz at center wavelength 800 nm. Using a 70:30 (R:T) beam splitter, the laser beam is divided into two parts: the stronger part with a fluence of 2.5 mJ/cm$^2$ and beam diameter of about 3 mm is used to pump the spintronic nanostructure (THz emitter), while the weaker part as a probe with power of 15 mW was transmitted through a computer-controlled delay (linear stage) to synchronize the pump and probe path and to excite a photoconductive antenna (BATOP optoelectronics) with a 180 $\mu$m dipole length as a detector of the generated THz pulse. The detection antenna exhibits dimensions of 5 $\mu$m and 10 $\mu$m for its gap and width, respectively (refer to the magnified section of Fig. 1(a)). An external magnetic field (20 mT) in the direction of the y-axis perpendicular to the incident pump beam direction is applied to the spintronic emitter to magnetize it and determine the generated THz wave polarization plane. The stronger optical beam (pump) is focused onto the sample from the non-magnetic layer by an aspherical lens with 11 mm focal length and then, THz emission is produced. Fig. 1(b, c) shows a schematic of the difference in the spatial divergence profile of THz emission produced by the FM|NM sample with and without the hyper-hemispherical lens. The generated conic THz beam is guided using two 90° silver-coated off-axis parabolic mirrors (OPM), with a focal lens of 6 cm, onto a silicon lens attached to the PCA chip located in the focal length of OPM. Detection of THz pulses takes place on the PCA chip and is performed using a balanced photodiode, optical chopper, and SR510 lock-in amplifier. The pump beam was modulated by an optical chopper at a frequency of 500

**Table 2.** Parameters used to ray tracing in COMSOL simulation.

| Name | Expression | Value | Description |
|---|---|---|---|
| $\mathbf{R}_{\mathrm{lens_S}}$ | 5 [mm] | 0.005 m | Radius of hyper-hemispherical lens of source |
| $\mathbf{n}_{\mathrm{Si}}$ | 3.417 | 3.417 | Refractive index of Si in THz region |
| $\mathbf{t}_{\mathrm{substrate}}$ | 0.5 [mm] | 5E-4 m | Thickness of substrate |
| $\mathbf{d}_{\mathrm{lens_S}}$ | $\mathrm{R_{lens_S}}.(1+\mathrm{n}_{\mathrm{Si\ or\ PTFE}}^{-1})$ | Depend on used lens | Distance d between emitter and lens tip |
| $\mathbf{L}_{\mathrm{S}}$ | $\mathrm{R_{lens_S}}.(1+\mathrm{n}_{\mathrm{Si\ or\ PTFE}})$ | Depend on used lens | Distance L from the tip of the lens to the virtual focus located behind the lens. |
| $\mathbf{R}_{\mathrm{lens_D}}$ | 6 [mm] | 0.006 m | Radius of hyper-hemispherical lens of detector |
| $\mathbf{d}_{\mathrm{lens_D}}$ | $\mathrm{R_{lens_D}}.(1+\mathrm{n}_{\mathrm{Si}}^{-1})$ | 0.0077559 m | Distance d between PCA chip and lens tip |
| $\mathbf{L}_{\mathrm{D}}$ | $\mathrm{R_{lens_S}}.(1+\mathrm{n}_{\mathrm{Si}})$ | 0.026502 m | Distance L from the tip of the Si lens to the virtual focus located behind the Si lens. |
| $\mathbf{t}_{\mathrm{GaAs}}$ | 0.6 [mm] | 6E-4 m | Thickness of GaAs |
| $\mathbf{n}_{\mathrm{MgO}}$ | 3.2 | 3.2 | Refractive index of MgO in THz region |
| $\mathbf{n}_{\mathrm{Al_2O_3}}$ | 3.07 | 3.07 | Refractive index of $Al_2O_3$ in THz region |
| $\mathbf{n}_{\mathrm{SiO_2}}$ | 1.95 | 1.95 | Refractive index of $SiO_2$ in THz region |
| $\mathbf{n}_{\mathrm{PET}}$ | 1.7 | 1.7 | Refractive index of PET in THz region |
| $\mathbf{n}_{\mathrm{PTFE}}$ | 1.43 | 1.43 | Refractive index of PTFE in 1 THz |
| $\mathbf{n}_{\mathrm{GaAs}}$ | 3.6 | 3.6 | Refractive index of Si-GaAs in THz region |

Hz. After the THz pulse and the probe beam are reached simultaneously by the delay stage, the detected voltage in the PCA chip can be swept which is proportional to the amplitude of the THz electric field.

### 2.2 Simulation

A 3D axisymmetric feature of COMSOL Multiphysics 6.1 was used for studying the index-matching effect on THz collection by PCA chip. The steps of simulation processing are highlighted in Table 1. The meshing in COMSOL was controlled for General Physics and selected as a predefined extremely-fine mesh size. The geometry of the emitter to detector part of our set-up, created using COMSOL Multiphysics and its Ray Optics Module, as well as, the mesh configuration of substrate, hyper-hemispherical lens, and PCA chip are shown in Fig. 2. As an initial step in the modeling process, the parameters utilized in this research were defined. Some of the parameters correspond to the element's value in the experimental set-up, and others are adapted from Refs. [24, 41–44], which is listed in Table 2. The operation principle is that a THz beam induced by FM—NM bilayer structures enters the substrate and is directed to the photoconductive antenna as a detector by two parabolic mirrors.

The geometry in component part, as a second step of processing, consists of two paraboloidal reflectors 3D, spheres, cylinders, and blocks. Fig. 1(d) illustrates the schematic dimensions of the hyper-hemispherical lens. The focal length of paraboloidal reflector, the distance between the two parabolic mirrors, and dimensions of PCA chip used for the experiment, were fixed at 60 mm, 250 mm and $4\times4$ $(\mathrm{mm})^2$, respectively. In the current simulation, the emitter and detector have been positioned at $\mathrm{x}=-60$ and $\mathrm{x}=-310$ in mm unit, respectively. The materials selected from the COMSOL database were magnesium monoxide, sapphire, silicon dioxide, poly-ethylene terephthalate (PET), silver, silicon, and gallium arsenide. The cone angle of the THz beam is assumed not to exceed 40 degrees. Specifically, we defined 20,000 rays in the simulation to study the behavior of light in the setup.

## 3. Results and discussion

The process of pumping the structure from the substrate side results in the emergence of supplementary reflections from the substrate-air interface, leading to significant oscillations in the corresponding THz spectra. The metal surface in our geometry functions as an anti-reflection coating for the THz beam, effectively quelling any reflections from the substrate surface. This portrays in Fig. 1(b) for a Ni|Pt

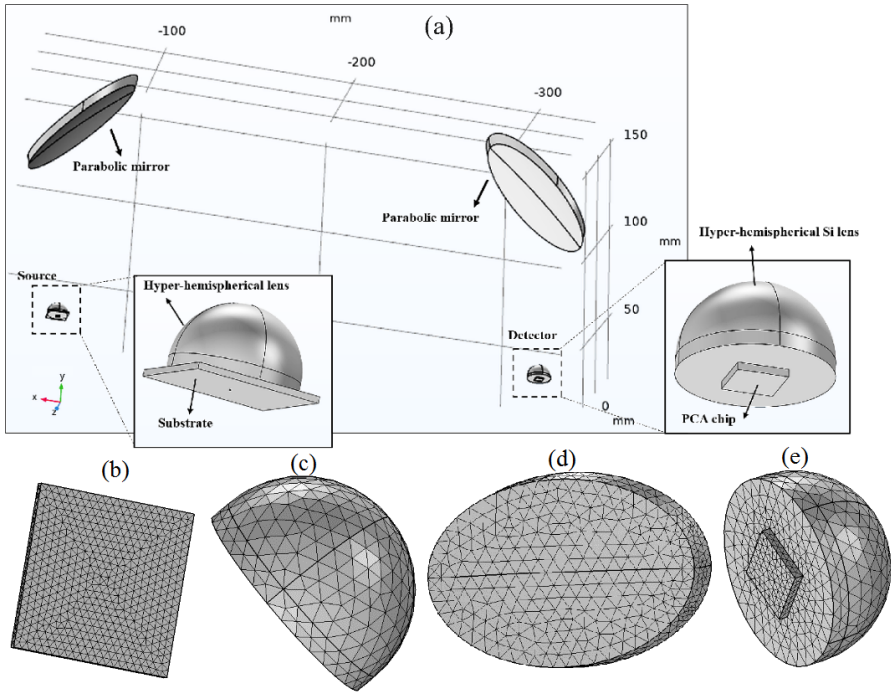


**Figure 2.** (a) Geometry used in the simulation. An extremely fine meshed view for (b) substrate, (c) hyper-hemispherical lens, (d) parabolic mirror, and (e) PCA chip attached to hyper-hemispherical Si lens.

sample on a MgO substrate in the absence of an attached silicon lens. A noisy pulse is shown in Fig. 3 for a 7 nm|6 nm Ni|Pt layer structure on 500 $\mu$m MgO substrate. From the analysis of the structure's output signal, it is evident that there is no trace of the THz signal. Indeed, the THz signal is diligently generated, yet regrettably eludes detection, presenting an intriguing challenge for further investigation about performance improvement of the THz-TDS setup. Although, a THz signal is observed in recent studies where the Ni|Pt structure, attached to the hyper-hemispherical Si lens and pumped on the substrate side [45] or the metal side rather than the MgO substrate [46], is examined. Also, THz emission from the Pt side for Fe|Pt sample grown on MgO substrate without the presence of a Si-lens has been reported [28].

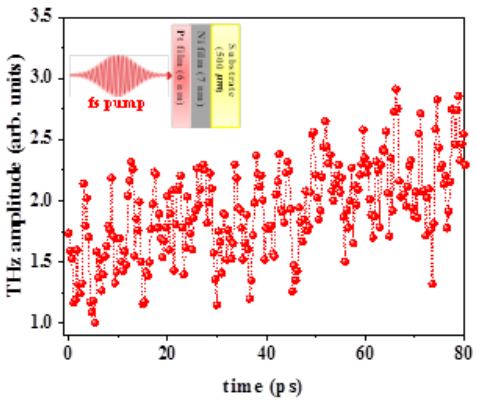


**Figure 3.** Signal collected from photoexcited Pt-capped Ni thin films grown on MgO substrate.

We investigated the remarkable impact of a hyper-hemispherical lens, when coupled with a THz emitter, on the THz collection capabilities of our THz-TDS system by harnessing the power of modeling ray-tracing with COMSOL to elucidate the factors contributing to the non-detection of THz emission. By carefully analyzing the number of rays that reached the PCA chip-air interface, we were able to gain valuable insights into the system's performance and make improvements that could lead to more accurate and sensitive measurements.

Figure 4 offers an insightful representation of the XY profiles for ray trajectories simulated which starts from the THz source (the FM|NM bilayer is capped on MgO substrate without a lens coupler) and terminates at the THz detector. Given our assumption of a cone angle of 40 degrees, the phenomenon of internal reflection manifests within the MgO substrate. This phenomenon arises due to the refraction theory for a planar surface that shows the boundary angle ($\alpha$) at which total internal reflection occurs can be determined by $\alpha = \sin^{-1}(1/n)$ [47, 48], where MgO exhibits a specific angle of 18.2°. Due to the high refractive index n $\sim$ 3.2

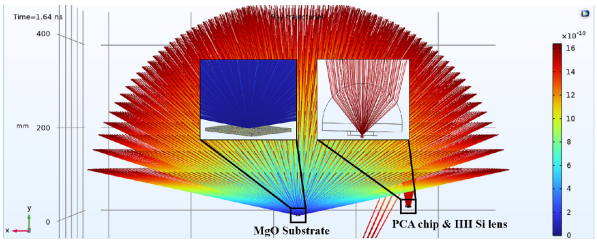


**Figure 4.** Snapshots showing ray trajectories through a MgO substrate of THz emitter.

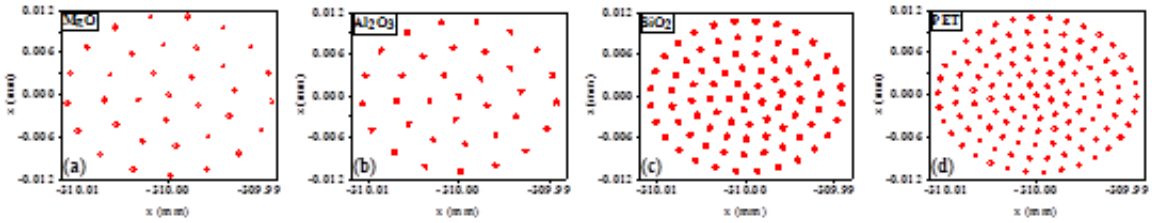


**Figure 5.** The intersection point result of simulation in the PCA chip-air interface for FM/NM bilayer grown on (a) MgO, (b) $Al_2O_3$, (c) $SiO_2$, and (d) PET substrate (in the absence of a hyper-hemispherical lens coupler).

of the MgO substrate, the THz waves emanating from the source are subject to significant diffraction at the interface between the substrate and the surrounding air medium, and only a minor proportion of the rays effectively make their way to the first and second parabolic mirrors, ultimately accumulating at the PCA chip.

The THz electric field is a powerful force that detects from the dynamic interplay of THz radiation with the antenna gap. To unlock its potential, one must skillfully calculate the number of rays that collect on the PCA chip and the expanse they cover. Figure 5 demonstrates the ray accumulation at the interface between the PCA chip and air. This image pertains to a scenario in which the THz emitter operates without the hyper-hemispherical lens coupler. Despite defining 20,000 THz rays, only a select few managed to make it to the antenna. The THz emitter layer deposited on MgO, $Al_2O_3$, $SiO_2$, and PET substrates allowed just 311, 347, 862, and 1138 rays, respectively, to reach their destination. Our simulation results confirm the non-detection of THz radiation in our experiment. Remarkably, as shown in Fig. 1(a), the antenna gap area is displayed at a smaller size of $5 \times 10\ \mu m^2$, yet the THz rays are concentrated into a larger $24 \times 24\ \mu m^2$ area on the PCA chip for all four substrates. The investigation revealed that the PET substrate, having a smaller difference in refractive index with air compared to the other substrates, offers a stronger THz collection capa-

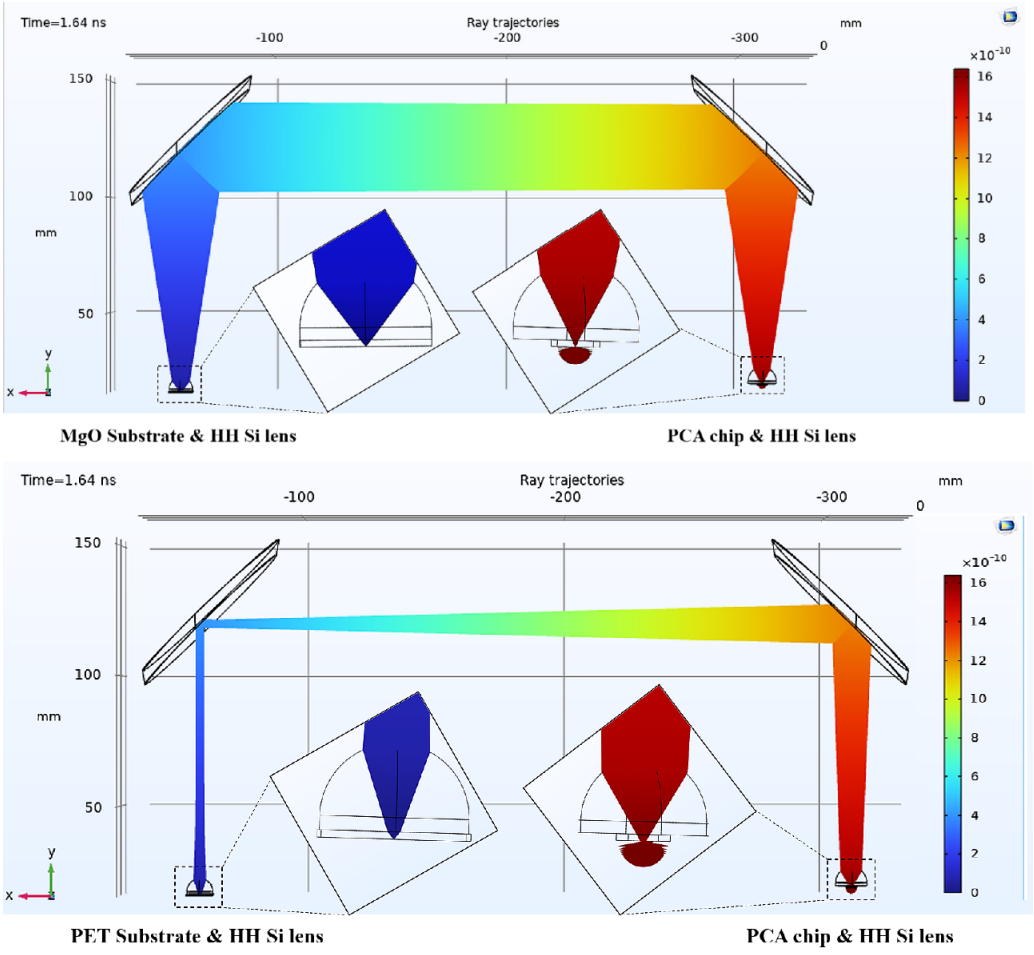


**Figure 6.** Snapshots showing ray trajectories through a hyper-hemispherical (HH) Si lens on (top) MgO, and (bottom) PET substrate.

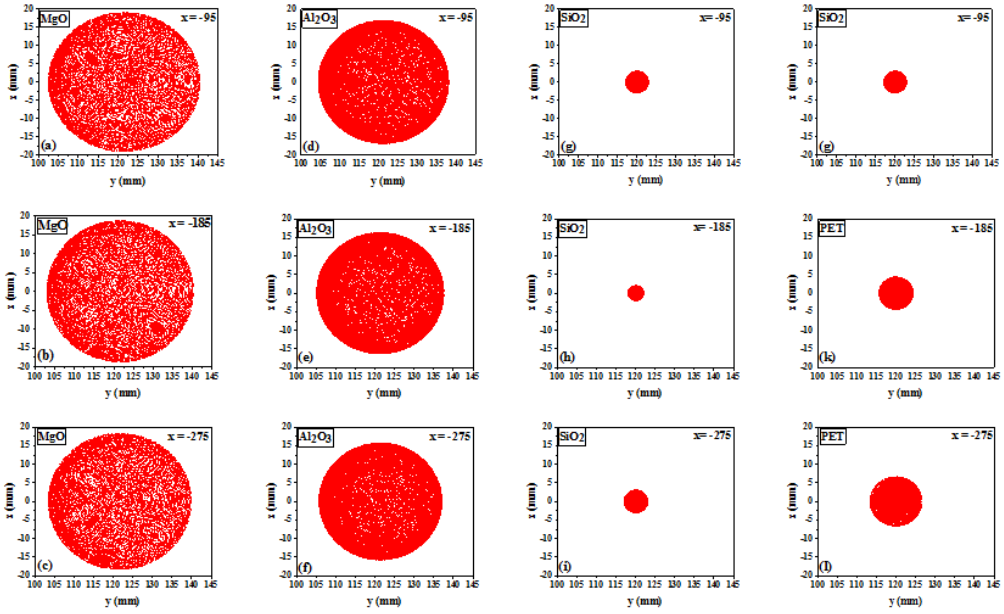


**Figure 7.** The intersection point result of simulation in the three parts of the beginning, middle and end between the two parabolic mirrors for the case where the Si hyper-hemispherical lens is attached to (a-c) MgO, (d-f) $Al_2O_3$, (g-i) $SiO_2$, and (j-l) PET substrate of THz emitter.

bility for the PCA chip.

To improve the THz collection efficiency, we conducted a simulation by incorporating the presence of a hyper-hemispherical lens attached to the substrate of STE. This allowed us to achieve superior performance and gain valuable insights into the THz-TDS system. Hyper-hemispherical lenses are a specialized type of common aspherical lens with a complex non-spherical shape that enables them to collect and focus light from a wide range of angles into a smaller area [49, 50]. It places the emitter at a position so that no rays are trapped by internal reflections [51]. This unique feature makes them ideal for high-resolution imaging systems, as they enhance the overall image quality and sensitivity of the system by collecting and focusing more light onto the sensor or detector [52]. In the first step, we have opted for a common hyper-hemispherical Si lens due to its similar refractive index to that of MgO or $Al_2O_3$ substrates. This choice is expected to yield superior results, as the close match in refractive index minimizes the likelihood of reflection and enables efficient transmission of THz radiation. The results of ray tracing simulations, as depicted in Figure 6, reveal that in the presence of a hyper-hemispherical Si lens coupler, THz emitters with MgO and PET substrate exhibit successful collection of all 20,000 rays by the antenna (the simulation results for the other two substrates are not presented in this particular step of the study).

The ray accumulation process in the y-z plane, between two parabolic mirrors, is depicted in Figure 7 for the three initial ($x = -95$), middle ($x = -185$), and final ($x = -275$) sections. Given that the y and z characteristics remain consistent across all three sections in the case of the MgO|FM|NM THz emitter, the resultant beam emerging from the second parabolic mirror can be effectively captured by the PCA surface at a short distance and subsequently collected. Conversely, when the emitter substrate is PET or $SiO_2$, the y and z coordinates in the three sections under consideration are not uniform. Therefore, it is anticipated that the rays will accumulate beyond the PCA gap surface, leading to weak detection signals.

While successful collection of all rays reaching the PCA chip is important, concentrating these rays within a smaller area of the PCA chip and within the antenna gap is crucial for achieving more powerful THz detection. The intersection point simulation results of THz radiation generated by a THz emitter in direct contact with a hyper-hemispherical silicon lens on the surface of the PCA chip are presented in Figure 8. Did you know that the distribution of gener-

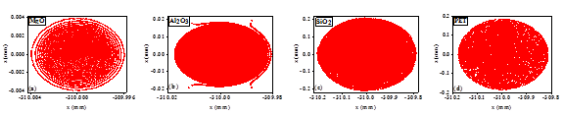

**Figure 8.** The intersection point result of simulation in the PCA chip-air interface for the case where the Si hyper-hemispherical lens is attached to (a) MgO, (b) $Al_2O_3$, (c) $SiO_2$, and (d) PET substrate of the THz emitter.

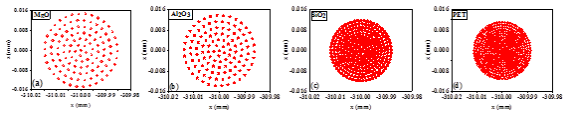

**Figure 9.** The intersection point result of simulation in the PCA chip-air interface for the case where the PTFE hyper-hemispherical lens is attached to (a) MgO, (b) $Al_2O_3$, (c) $SiO_2$, and (d) PET substrate of THz emitter.

ated THz radiation varies based on the substrate coating of the emitter? Our findings reveal that when the THz emitter is coated on the MgO, $Al_2O_3$, $SiO_2$, and PET substrates, the generated THz ray accumulates in different areas of the antenna surface, ranging from $8 \times 8$ to $400 \times 400$ $\mu m^2$. Our investigation has revealed that the MgO substrate, which concentrates THz radiation in an area of $8 \times 8$ $\mu m^2$ in the center of the chip, is the most effective substrate for directing all THz radiation to the PCA, among the substrates examined. The experimental results confirm that the MgO|FM|NM heterostructures produce a stronger THz pulse compared to $Al_2O_3$|FM|NM [28, 34]. The amplitude of the THz emission from the PET|FM|NM structure is found to be comparable to that of the $SiO_2$|FM|NM structure, consistent with experimental observations [53].

The attachment of a Teflon (PTFE) lens, which warrants careful consideration, was proposed in the next step due to the cost-effectiveness and ease of access to its raw materials that make it an attractive option for a wide range of applications [54, 55]. Figure 9 provides a visual representation of the accumulation of rays on the surface of the PCA chip when the THz source is coupled with a hyper-hemispherical Teflon lens. In this case, we observe a slight improvement compared to STE without a lens coupler; where among the 20,000 defined rays, the THz emitter grown on MgO, $Al_2O_3$, $SiO_2$, and PET substrates (hyper-hemispherical Teflon lens attachment) exhibits selective propagation, with only 1208, 1346, 3500, and 4699 rays successfully reaching the first parabolic mirror. Subsequently, these rays efficiently traverse the second parabolic mirror and ultimately reach the surface of the PCA chip, where they are collected. By applying Snell's law ($n_1 \sin\theta_1 = n_2 \sin\theta_2$), we've discovered that PET and $SiO_2$ substrates have a lower chance of experiencing internal reflection, leading to a more concentrated THz radiation on the PCA chip's surface and enhanced collection efficiency, compared to MgO and $Al_2O_3$ substrates. Our findings indicate that when the MgO|FM|NM heterostructure operates without a hyper-hemispherical lens coupler, the PC antenna collects only 1.55% of THz rays. With the use of a hyper-hemispherical Teflon lens attached to the MgO|FM|NM heterostructure, collection efficiency increases to only 6%, which is insufficient to achieve strong detection of weak THz radiation. However, the PET|FM|NM heterostructure increases collection efficiency from 5.69% (without lens coupler) to 23.49% (with Teflon lens coupler). Consequently, a PET substrate with a Teflon hyper-hemispherical lens coupler could be a favorable environment for improved collection efficiency of STE-induced THz radiation, in the absence of Si-lens.

## 4. Conclusion

To summarize, we did not detect any spintronic THz emission from a Ni|Pt bilayer structure (without lens coupler) that was grown on a MgO substrate via sputtering deposition. To explore the conditions required for the detection of THz radiation in the common STE, we conducted simulations using the COMSOL Ray Optics Module. In addition to substrate engineering, we also investigated the impact of hyper-hemispherical lens attachment on the THz radiation collection efficiency. The COMSOL analysis shows that when a weak STE without a lens coupler, the same as Ni|Pt, is pumped from the side of the metal layer, a small percentage of THz rays are collected on the PCA chip. However, the use of hyper-hemispherical Si-lens in direct contact with the substrate|FM|NM structure provides a significant improvement in the collection efficiency of THz emission. Approximately 64.5 times enhancement in the THz emission collection efficiency from NM|FM|MgO-substrate was confirmed by the attachment of the hyper-hemispherical Si-lens compared to that without the Si-lens coupler. However, the coupling of a hyper-hemispherical Teflon-lens to the structure does not improve emission collection efficiency as much as a Si-lens coupler, but it can be a suitable option for the PET substrate in the lack of a Si-lens coupler. These findings highlight the importance of careful selection of optical components in THz technology and may inform the development of advanced THz devices and systems for a range of applications in materials science, biomedical imaging, spectroscopy, and beyond in the THz spectral range.

**Acknowledgments**
This work was supported by **Iranian National Science Foundation** by number **98002631**.

**Ethical approval**
This manuscript does not report on or involve the use of any animal or human data or tissue. So the ethical approval is not applicable.

**Authors Contributions**
S. M. Hosseini write the main text. Measurement setup and simulation were done with S. M. Hosseini and A. Sadraei Javaheri. F. Jahangiri, S. M. Hamidi, and H. Latifi supervised the work and read the final text of the manuscript.

**Availability of data and materials**
The datasets used and/or analyzed during the current study available from the corresponding author.

**Conflict of Interests**
The authors declare that they have no known competing financial interests or personal relationships that could have appeared to influence the work reported in this paper.

## References

[1] I. Malhotra and G. Singh. *"Terahertz Terahertz (THz) Technology for Biomedical Application Biomedical applications"*, volume . Springer, 2021.

[2] J. Zhong, X. Xu, and Y.-S. Lin. "Tunable terahertz metamaterial with electromagnetically induced transparency characteristic for sensing application". *Nanomaterials*, **11**:2175, 2021.

[3] M. Walther, B. M. Fischer, A. Ortner, A. Bitzer, A. Thoman, and H. Helm. "Chemical sensing and imaging with pulsed terahertz radiation". *Analytical and Bioanalytical Chemistry*, **397**:1009–1017, 2010.

[4] Y. Wen, J. Delin, M. Wei, F. Yun, L. Ming, D. Liquan, Z. Yuejin, and Y. Xiaomei. "Photomechanical meta-molecule array for real-time terahertz imaging". *Microsystems & Nanoengineering*, **3**:1–7, 2017.

[5] S. Ergün and S. Sönmez. "Terahertz technology for military applications". *Journal of Management and Information Science*, **3**:13–16, 2015.

[6] I. F. Akyildiz, A. Kak, and S. Nie. "6G and beyond: The future of wireless communications systems". *IEEE Access*, **8**:133995–134030, 2020.

[7] T. Amini, F. Jahangiri, Z. Ameri, and M. A. Hemmatian. "A review of feasible applications of THz waves in medical diagnostics and treatments". *Journal of Lasers in Medical Sciences*, **12**, 2021.

[8] S. Huang, Y. Wang, D. Yeung, A. Ahuja, Y. Zhang, and E. Pickwell-MacPherson. "Tissue characterization using terahertz pulsed imaging in reflection geometry". *Physics in Medicine & Biology*, **54**:149, 2008.

[9] L. Yu, L. Hao, T. Meiqiong, H. Jiaoqi, L. Wei, D. Jinying, C. Xueping, F. Weiling, and Z. Yang. "The medical application of terahertz technology in non-invasive detection of cells and tissues: opportunities and challenges". *RSC Advances*, **9**:9354–9363, 2019.

[10] M. Hibberd, D. Lake, N. Johansson, T. Thomson, S. Jamison, and D. Graham. "Magnetic-field tailoring of the terahertz polarization emitted from a spintronic source". *Applied Physics Letters*, **114**, 2019.

[11] T. S. Seifert, N. M. Tran, O. Gueckstock, S. M. Rouzegar, L. Nadvornik, S. Jaiswal, G. Jakob, V. V. Temnov, M. Münzenberg, M. Wolf, M. Kläui, and T. Kampfrath. "Terahertz spectroscopy for all-optical spintronic characterization of the spin-Hall-effect metals Pt, W and Cu80Ir20". *Journal of Physics D: Applied Physics*, **51**:364003, 2018.

[12] O. Gueckstock, L. Nadvornik, M. Gradhand, T. S. Seifert, G. Bierhance, R. Rouzegar, M. Wolf, M. Vafaee, J. Cramer, M-A. Syskaki, et al. "Terahertz spin-to-charge conversion by interfacial skew scattering in metallic bilayers". *Advanced Materials*, **33**:2006281, 2021.

[13] W. Zhang, P. Maldonado, Z. Jin, T. S. Seifert, J. Arabski, G. Schmerber, E. Beaurepaire, M. Bonn, T. Kampfrath, P. M. Oppeneer, and D. Turchinovich. "Ultrafast terahertz magnetometry". *IEEE Photonics Journal*, **5**:4800806, 2013. DOI: https://doi.org/10.1109/JPHOT.2013.2288298.

[14] G. Li, R. Mikhaylovskiy, K. Grishunin, J. Costa, T. Rasing, and A. Kimel. "Laser induced THz emission from femtosecond photocurrents in Co/ZnO/Pt and Co/Cu/Pt multilayers". *Journal of Physics D: Applied Physics*, **51**:134001, 2018.

[15] T. Amini and F. Jahangiri. "Regenerative terahertz wave parametric amplifier based on four-wave mixing in asynchronously pumped graphene oxide integrated TOPAS". *Optics Express*, **29**:33053–33066, 2021.

[16] T. Amini and F. Jahangiri. "Optimized design for a terahertz parametric oscillator based on degenerate four-wave mixing in silicon nitride". *JOSA B*, **37**: 2155–2157, 2020.

[17] H. Dang, J. Hawecker, E. Rongione, G. Baez Flores, D. Quang To, Juan C. R. Sánchez, H. Nong J. Mangeney, J. Tignon, F. Godel, et al. "Ultrafast spin-currents and charge conversion at 3d-5d interfaces probed by time-domain terahertz spectroscopy". *Applied Physics Reviews*, **7**, 2020.

[18] J. Walowski and M. Münzenberg. "Perspective: Ultrafast magnetism and THz spintronics". *Journal of Applied Physics*, **120**, 2016.

[19] S. M. Hosseini, F. Jahangiri, R. Jalilian, and S. Hamidi. "Comparative study of femtosecond laser-induced ultrafast magnetization dynamics in soft ferromagnetic ultra-thin alloy". *Journal of Magnetism and Magnetic Materials*, **579**:170879, 2023.

[20] T. Seifert, S. Jaiswal, U. Martens, J. Hannegan, L. Braun, P. Maldonado, F. Freimuth, A. Kronenberg, J. Henrizi, I. Radu, et al. "Efficient metallic spintronic emitters of ultrabroadband terahertz radiation". *Nature Photonics*, **10**:483–488, 2016.

[21] T. Seifert, S. Jaiswal, M. Sajadi, G. Jakob, S. Winnerl, M. Wolf, M. Kläui, and T. Kampfrath. "Ultrabroadband single-cycle terahertz pulses with peak fields

of 300 kV $cm^{-1}$ from a metallic spintronic emitter". *Applied Physics Letters*, **110**, 2017.

[22] T. S. Seifert, L. Cheng, Z. Wei, T. Kampfrath, and J. Qi. "Spintronic sources of ultrashort terahertz electromagnetic pulses". *Applied Physics Letters*, **120**, 2022.

[23] R. Gupta, S. Husain, A. Kumar, R. Brucas, A. Rydberg, and P. Svedlindh. "$Co_2FeAl$ full Heusler compound based spintronic terahertz emitter". *Advanced Optical Materials*, **9**:2001987, 2021.

[24] Y. Ni, Z. Jin, B. Song, X. Zhou, H. Chen, C. Song, Y. Pang, C. Zhang, F. Pan, G. Ma, Y. Zhu, and S. Zhuang. "Temperature-Dependent Terahertz Emission from $Co/Mn_2Au$ Spintronic Bilayers". *Physica Status Solidi (RRL)–Rapid Research Letters*, **15**: 2100290, 2021.

[25] M. Nakajima, K. Uchida, M. Tani, and M. Hangyo. "Strong enhancement of terahertz radiation from semiconductor surfaces using MgO hemispherical lens coupler". *Applied Physics Letters*, **85**:191–193, 2004.

[26] R. Gupta, E. Bagherikorani, V. Mottamchetty, M. Pavelka, K. Jatkar, D. Dancila, K. Mohammadpour-Aghdam, A. Rydberg, R. Brucas, H. A. Durr, and P. Svedlindh. "Strain engineering of epitaxial Pt/Fe spintronic terahertz emitter". *arXiv preprint*, : arXiv:2110.01547, 2021.

[27] H. Zhang, Z. Feng, J. Zhang, H. Bai, H. Yang, J. Cai, W. Zhao, W. Tan, F. Hu, B. Shen, and J. Sun. "Laser pulse induced efficient terahertz emission from Co/Al heterostructures". *Physical Review B*, **102**:024435, 2020.

[28] D. M. Nenno, L. Scheuer, D. Sokoluk, S. Keller, G. Torosyan, A. Brodyanski, J. Lösch, M. Battiato, et al. "Modification of spintronic terahertz emitter performance through defect engineering". *Scientific Reports*, **9**:13348, 2019.

[29] C. C. Renaud, M. Natrella, C. Graham, J. Seddon, F. Van Dijk, and A. J. Seeds. "Antenna integrated THz uni-traveling carrier photodiodes". *IEEE Journal of Selected Topics in Quantum Electronics*, **24**:1–11, 2017.

[30] K. Çınar, H. Altan, and A. Şahin. *"THz transmission and detection through glow discharge detectors"*, volume **8716**. SPIE, 2013.

[31] Z. B. Harris, S. Katletz, M. E. Khani, A. Virk, and M. H. Arbab. "Design and characterization of telecentric f-$\theta$ scanning lenses for broadband terahertz frequency systems". *AIP Advances*, **10**, 2020.

[32] W. Li, F. Qi, Y. Wang, P. Liu, and Z. Liu. "Refractive aspherical lens for terahertz imaging". *Optics Communications*, **433**:14–17, 2019.

[33] T. Vogel, A. Omar, S. Mansourzadeh, F. Wulf, N. Martin Sabanes, M. Müller, T. S. Seifert, A. Weigel, et al. "Average power scaling of THz spintronic emitters efficiently cooled in reflection geometry". *Optics Express*, **30**:20451–20468, 2022.

[34] G. Torosyan, S. Keller, L. Scheuer, R. Beigang, and E. T. Papaioannou. "Optimized spintronic terahertz emitters based on epitaxial grown Fe/Pt layer structures". *Scientific Reports*, **8**:1311, 2018.

[35] V. K. Mag-usara, G. Torosyan, M. Talara, J. Afalla, J. E. Muldera, H. Kitahara, L. Scheuer, E. Th. Papaioannou, and M. Tani. "Optical excitation wavelength-independent terahertz generation using an optimized spintronic bilayer". *J. Jpn. Soc. Infrared Science & Technology*, **29**:13–16, 2020.

[36] D. G. Cooke. "Time-resolved terahertz spectroscopy of bulk and nanoscale semiconductors". *Thesis (Ph.D.). University of Alberta (Canada)*, , 2007.

[37] U. Nandi, M. S. Abdelaziz, S. Jaiswal, G. Jakob, O. Gueckstock, R. Rouzegar, T. S. Seifert, M. Kläui, T. Kampfrath, and S. Preu. "Antenna-coupled spintronic terahertz emitters driven by a 1550 nm femtosecond laser oscillator". *Applied Physics Letters*, **115**, 2019.

[38] M. Talara, D. S. Bulgarevich, C. Tachioka, V. K. Mag-usara, J. Muldera, T. Furuya, H. Kitahara, M. Clare Escaño, et al. "Efficient terahertz wave generation of diabolo-shaped Fe/Pt spintronic antennas driven by a 780 nm pump beam". *Applied Physics Express*, **14**: 042008, 2021.

[39] L. Scheuer, M. Ruhwedel, D. Karfaridis, I. G. Vasileiadis, D. Sokoluk, G. Torosyan, G. Vourlias, G. P. Dimitrakopoulos, M. Rahm, et al. "THz emission from Fe/Pt spintronic emitters with L10-FePt alloyed interface". *Iscience*, **25**, 2022.

[40] L. Scheuer, M. Ruhwedel, G. Torosyan, R. Beigang, G. Schmidt, and E. T. Papaioannou. "Correlation of interface transmission in THz spintronic emitters with spin mixing conductance in spin pumping experiments". *Spintronics XIII*, **114**:64–71, 2020.

[41] C. Liu, S. Wang, S. Zhang, Q. Cai, P. Wang, Q. Cai, P. Wang, C. Tain, L. Zhou, Y. Wu, and Z. Tao. "Active spintronic-metasurface terahertz emitters with tunable chirality". *Advanced Photonics*, **3**:056002–056002, 2021.

[42] B. Zhou, M. Rasmussen, P. Rebsdorf Whelan, J. Ji, A. Shivayogimath, P. Bøggild, and P. U. Jepsen. "Non-Linear Conductivity Response of Graphene on Thin-Film PET Characterized by Transmission and Reflection Air-Plasma THz-TDS". *Sensors*, **23**:3669, 2023.

[43] 2009 Y.-S. Lee, . *"Principles of terahertz science and technology"*, volume . Springer Science & Business Media, 2009.

[44] H. Yasuda and I. Hosako. "Measurement of terahertz refractive index of metal with terahertz time-domain spectroscopy". *Japanese Journal of Applied Physics*, **47**:1632, 2008.

[45] J. P. Ferrolino, N. I. Cabello, A. De Los Reyes, H. Bardolaza, I. C. Verona, V. K. Mag-usara, J. P. Afalla, M. Talara, H. Kitahara, et al. "Thickness dependence of the spintronic terahertz emission from Ni/Pt bilayer grown on MgO via electron beam deposition". *Applied Physics Express*, **14**:093001, 2021.

[46] J. P. Ferrolino, N. I. Cabello, A. De Los Reyes, V. K. Mag-Usara, J. P. Afalla, H. Bardaloza, I. C. Verona, M. Talara, H. Kitahara, et al. "Spintronic terahertz emission from Ni/Pt bilayer grown on MgO". *Journal of Physics: Conference Series, IOP Publishing*, **1943**: 01203, 2021.

[47] C. Que and E. Estacio. "Terahertz emission enhancement using a metallic hole on a SI-GaAs semiconductor". **12**:200–203, 2010.

[48] M. B. Johnston, D. M. Whittaker, A. Dowd, A. G. Davies, E. H. Linfield, X. Li, and D. A. Ritchie. "Generation of high-power terahertz pulses in a prism". *Optics Letters*, **27**:1935–1937, 2002.

[49] C. Fattinger and D. Grischkowsky. "Terahertz beams". *Applied Physics Letters*, **54**:490–492, 1989.

[50] D. M. Mittleman, R. H. Jacobsen, and M. C. Nuss. "T-ray imaging". *IEEE Journal of Selected Topics in Quantum Electronics*, **2**:679–692, 1996.

[51] J. Van Rudd and D. M. Mittleman. "Influence of substrate-lens design in terahertz time-domain spectroscopy". *Journal of the Optical Society of America B*, **19**:319–329, 2002.

[52] R. Zatta, R. Jain, J. Grzyb, and U. R. Pfeiffer. "Resolution limits of hyper-hemispherical silicon lens-integrated THz cameras employing geometrical multi-frame super-resolution imaging". *IEEE Transactions on Terahertz Science and Technology*, **11**:277–286, 2021.

[53] Z. Jin, Y. Peng, Y. Ni, G. Wu, B. Ji, X. Wu, Z. Zhang, G. Ma, C. Zhang, L. Chen, A. V. Balakin, et al. "Cascaded amplification and manipulation of terahertz emission by flexible spintronic heterostructures". *Laser & Photonics Reviews*, **16**:2100688, 2022.

[54] H. Feng, D. An, H. Tu, W. Bu, W. Wang, Y. Zhang, H. Zhang, X. Meng, et al. "A passive video-rate terahertz human body imager with real-time calibration for security applications". *Applied Physics B*, **126**:143, 2020.

[55] K. Kuroo, R. Hasegawa, T. Tanabe, and Y. Oyama. "Terahertz Application for non-destructive inspection of coated Al electrical conductive wires". *Journal of Imaging*, **3**:27, 2017.